

# Photonic crystal formation on optical nanofibers using femtosecond laser ablation technique

K. P. Nayak\* and K. Hakuta

Center for Photonic Innovations, University of Electro-Communications,  
Tokyo 182-8585, Japan

\*kali@cpi.uec.ac.jp

**Abstract:** We demonstrate that thousands of periodic nano-craters are fabricated on a subwavelength-diameter tapered optical fiber, an optical nanofiber, by irradiating with just a single femtosecond laser pulse. A key aspect of the fabrication is that the nanofiber itself acts as a cylindrical lens and focuses the femtosecond laser beam on its shadow surface. We also demonstrate that such periodic structures on the nanofiber, act as a 1-D photonic crystal (PhC). Such PhC structures on the nanofiber will strongly enhance the field confinement in such a tapered fiber-based system and may open new avenues in nanophotonics and quantum information technology.

---

## References and links

1. J. Vuckovic, M. Loncar, H. Mabuchi, and A. Scherer, "Design of photonic crystal microcavities for cavity QED," *Phys. Rev. E* **65**, 016608 (2001).
2. J. S. Foresi, P. R. Villeneuve, J. Ferrera, E. R. Thoen, G. Steinmeyer, S. Fan, J. D. Joannopoulos, L. C. Kimerling, H. I. Smith, and E. P. Ippen, "Photonic-bandgap microcavities in optical waveguides," *Nature* **390**, 143-145 (1997).
3. M. Eichenfield, R. Camacho, J. Chan, K. J. Vahala, and O. Painter, "A picogram- and nanometre-scale photonic-crystal optomechanical cavity," *Nature* **459**, 550-555 (2009).
4. O. Painter, R. K. Lee, A. Scherer, A. Yariv, J. D. O'Brien, P. D. Dapkus, and I. Kim, "Two-dimensional photonic band-gap defect mode laser," *Science* **284**, 1819-1821 (1999).
5. M. Loncar, A. Scherer, and Y. Qiu, "Photonic crystal laser sources for chemical detection," *Appl. Phys. Lett.* **82**, 4648-4650 (2003).
6. T. Tanabe, M. Notomi, S. Mitsugi, A. Shinya, and E. Kuramochi, "All-optical switches on a silicon chip realized using photonic crystal nanocavities," *Appl. Phys. Lett.* **87**, 151112 (2005).
7. T. Yoshie, A. Scherer, J. Hendrickson, G. Khitrova, H. M. Gibbs, G. Rupper, C. Ell, O. B. Shchekin, and D. G. Deppe, "Vacuum Rabi splitting with a single quantum dot in a photonic crystal nanocavity," *Nature* **432**, 200-203 (2004).
8. K. Hennessy, A. Badolato, M. Winger, D. Gerace, M. Atature, S. Gulde, S. Falt, E. L. Hu, and A. Imamoglu, "Quantum nature of a strongly coupled single quantum dot-cavity system," *Nature* **445**, 896-899 (2007).
9. M. Toishi, D. Englund, A. Faraon, and J. Vuckovic, "High-brightness single photon source from a quantum dot in a directional-emission nanocavity," *Opt. Express* **17**, 14618-14626 (2009).
10. D. Englund, B. Shields, K. Rivoire, F. Hatami, J. Vuckovic, H. Park, and M. D. Lukin, "Deterministic coupling of a single nitrogen vacancy center to a photonic crystal cavity," *Nano Lett.* **10**, 3922-3926 (2010).
11. K. P. Nayak, P. N. Melentiev, M. Morinaga, F. L. Kien, V. I. Balykin, and K. Hakuta, "Optical nanofiber as an efficient tool for manipulating and probing atomic Fluorescence," *Opt. Express* **15**, 5431-5438 (2007).
12. K. P. Nayak and K. Hakuta, "Single atoms on an optical nanofibre," *New J. Phys.* **10**, 053003 (2008).
13. R. Yalla, K. P. Nayak, and K. Hakuta, "Fluorescence photon measurements from single quantum dots on an optical nanofiber," *Opt. Express* **20**, 2932-2941 (2012).
14. F. L. Kien, S. Dutta Gupta, V. I. Balykin, and K. Hakuta, "Spontaneous emission of a cesium atom near a nanofiber: Efficient coupling of light to guided modes," *Phys. Rev. A* **72**, 032509 (2005).
15. R. Yalla, F. L. Kien, M. Morinaga, and K. Hakuta, "Efficient channeling of fluorescence photons from single quantum dots into guided modes of optical nanofiber," *Phys. Rev. Lett.* **109**, 063602 (2012).
16. F. L. Kien, V. I. Balykin, and K. Hakuta, "Scattering of an evanescent light field by a single cesium atom near a nanofiber," *Phys. Rev. A* **73**, 013819 (2006).

17. F. L. Kien, V. I. Balykin, and K. Hakuta, "Atom trap and waveguide using a two-color evanescent light field around a subwavelength-diameter optical fiber," *Phys. Rev. A* **70**, 063403 (2004).
  18. E. Vetsch, D. Reitz, G. Sagué, R. Schmidt, S. T. Dawkins, and A. Rauschenbeutel, "Optical interface created by laser-cooled atoms trapped in the evanescent field surrounding an optical nanofiber," *Phys. Rev. Lett.* **104**, 203603 (2010).
  19. A. Goban, K. S. Choi, D. J. Alton, D. Ding, C. Lacroûte, M. Pototschnig, T. Thiele, N. P. Stern, and H. J. Kimble, "Demonstration of a state-insensitive, compensated nanofiber trap," *Phys. Rev. Lett.* **109**, 033603 (2012).
  20. F. L. Kien and K. Hakuta, "Cavity-enhanced channeling of emission from an atom into a nanofiber," *Phys. Rev. A* **80**, 053826 (2009).
  21. H. J. Kimble, "The quantum internet," *Nature* **453**, 1023-1030 (2008).
  22. M. Becker, J. Bergmann, S. Brückner, M. Franke, E. Lindner, M. W. Rothhardt, and H. Bartelt, "Fiber Bragg grating inscription combining DUV sub-picosecond laser pulses and two-beam interferometry," *Opt. Express* **16**, 19169-19178 (2008).
  23. H. C. van de Hulst, *Light Scattering by Small Particles* (Dover Publication Inc., New York, 1981) pp 297-328.
  24. F. L. Kien and K. Hakuta, "Microtraps for atoms outside a fiber illuminated perpendicular to its axis: Numerical results," *Phys. Rev. A* **80**, 013415 (2009).
  25. S. J. Mihailov, D. Grobnc, C. W. Smelser, P. Lu, R. B. Walker, and H. Ding, "Induced Bragg gratings in optical fibers and waveguides using an ultrafast infrared laser and a phase mask," *Laser Chem.* **2008**, 416251 (2008).
  26. C. W. Smelser, S. J. Mihailov, and D. Grobnc, "Formation of Type I-IR and Type II-IR gratings with an ultrafast IR laser and a phase mask," *Opt. Express* **13**, 5377-5386 (2005).
  27. K. P. Nayak, F. L. Kien, Y. Kawai, K. Hakuta, K. Nakajima, H. T. Miyazaki, and Y. Sugimoto, "Cavity formation on an optical nanofiber using focused ion beam milling technique," *Opt. Express* **19**, 14040-14050 (2011).
  28. F. L. Kien, K. P. Nayak, and K. Hakuta, "Nanofibers with Bragg gratings from equidistant holes," *J. Modern Opt.* **59**, 274-286 (2012).
- 

## 1. Introduction

Confinement of light to wavelength-scale volumes possesses important implications to control the light-matter interactions at single photon and single emitter level. The emerging field of nanofabrication technology has encouraged various designs of micro/nano-photonic structures to be investigated. In particular 2-D [1] and 1-D [2, 3] photonic crystal (PhC) structures have enabled new prospects in nanolasers [4], chemical sensing [5] and optical switching [6]. Moreover, the strong light-matter coupling [7, 8, 9, 10] in these PhC structures, has opened new avenues for quantum information technology. However, integrating these PhC structures to fiber-based communication channels still remains challenging. In this context, tapered optical fibers with subwavelength diameters, known as optical nanofibers, may provide a promising platform for realizing strong light-matter interaction in a fiber-based system.

In recent years, optical nanofibers have opened a new paradigm in manipulating single/few-atom fluorescence [11, 12, 13]. A nanofiber is realized by adiabatically tapering a conventional single mode optical fiber which enables light in the fundamental mode to be coupled in and out of the nanofiber with more than 95% efficiency. Due to the subwavelength diameter the field in the guided mode is strongly confined in the transverse direction. As a result the spontaneous emission of atoms can be strongly modified around the nanofiber and an appreciable amount of atomic fluorescence can be coupled to the guided modes [14, 15]. Also the strong evanescent tail of the guided field gives excellent access for trapping and probing few atoms around the nanofiber [16, 17, 18, 19].

The light-matter coupling in such nanofiber system can be substantially improved by fabricating a 1-D PhC structure on the nanofiber. The PhC structure provides longitudinal confinement of the field in the nanofiber guided modes. Due to the strong transverse confinement of the nanofiber guided modes, the coupling between the atom and the guided modes will be significantly enhanced and the strong-coupling regime can be realized, even for moderate finesse [20]. Such PhC nanofiber system may become a promising workbench for quantum non-linear optics and may serve as nodes in quantum networks [21]. Also the PhC nanofibers may open up exciting new applications in lasing, optical switching and chemical/biological sensing.

In this paper, we present the fabrication of PhC nanofibers using a femtosecond laser ablation technique. We demonstrate that thousands of periodic nano-craters are fabricated on optical nanofibers by irradiating with just a single femtosecond laser pulse. A key aspect of the fabrication is the lensing effect of the nanofiber itself. We also demonstrate that such periodic nano-craters on the nanofiber, induce strong modulation of refractive index and act as a 1-D PhC.

## 2. Experiments

### 2.1. Fabrication setup

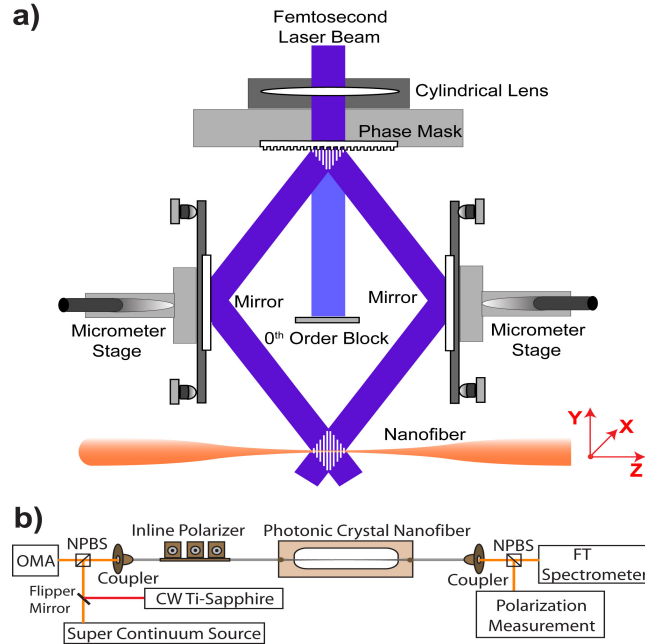


Fig. 1. (Color online) (a) The schematic diagram of the fabrication setup. The phase mask splits the femtosecond laser beam into  $\pm$  first orders which are then recombined by the folding mirrors to create an interference pattern at the nanofiber. A cylindrical lens is used to line focus the femtosecond laser along the nanofiber. A zero order block is used to avoid any residual zero order light in the interference region. (b) The schematic diagram of the optical measurements. The transmission and reflection spectra of the fabricated nanofiber samples are simultaneously measured by varying the polarization of the input light (see text for details). NPBS and OMA denote non-polarizing beam splitter and optical multi-channel analyzer, respectively.

A schematic diagram of the fabrication setup is shown in Fig. 1(a). The femtosecond laser (Coherent Libra-HE) used for the fabrication has a central wavelength ( $\lambda$ ) of 400 nm and generates 120 fs pulses at a repetition rate of 1 kHz with maximum pulse energy of 1.3 mJ. A Talbot interferometer [22], consisting of a phase mask as beam splitter and two folding mirrors, is built to create the two-beam interference pattern on the nanofiber. The phase mask used for the fabrication has a uniform pitch ( $\Lambda_p$ ) of 700 nm and was designed for zero order suppression at 400 nm wavelength. The position of the folding mirrors is carefully chosen to symmetrically recombine the first orders at the nanofiber position, thereby creating an interference pattern with

a period of  $\Lambda_p/2 = 350$  nm. A cylindrical lens is used to line-focus the femtosecond laser beam along the nanofiber. The typical  $1/e^2$  beam size at the nanofiber is  $5.4 \text{ mm} \times 60 \text{ }\mu\text{m}$ . The polarization of the femtosecond laser beam is perpendicular to the nanofiber axis. Tapered nanofibers with waist diameters ( $2a$ ) of 450-650 nm are used for the fabrication. After the fabrication, the nanofiber samples are observed using a scanning electron microscope (SEM).

## 2.2. Alignment of the fabrication setup

The interferometer alignment is highly sensitive to the optical path length difference between the two first orders. The path length difference must be smaller than  $36 \text{ }\mu\text{m}$  as the spatial overlap is limited by the femtosecond laser pulse width [22, 25]. Hence, the positions of the folding mirrors are controlled by micrometer stages and the mirror tilt angles are precisely controlled. The alignment of the interferometer is performed by observing the periodic ablation pattern on a glass plate, using the SEM. After alignment of the interferometer, the glass plate is replaced by the tapered nanofiber. For the fabrication, the tapered fiber is mounted on a metallic holder having a central hole of 6 cm length, so that the nanofiber is protected from contamination due to ablation of the substrate. The overlap of the femtosecond laser beam with the nanofiber is monitored by reducing the pulse energy to minimum value and observing the scattered light from the nanofiber using a CCD camera. Maximum overlap is achieved using a X-stage and a rotation-stage.

## 2.3. Measurement of optical properties

The optical properties of the fabricated samples are characterized by measuring the transmission and reflection spectra. A schematic of the experimental setup is shown in Fig. 1(b). A supercontinuum light source (SuperK Extreme, NKT Photonics) is launched into the tapered fiber sample and the spectrum of the transmitted light is measured using a Fourier transform spectrometer (FT-spectrometer). The resolution of the FT-spectrometer (Nicolet 8700, Thermo Fisher Scientific) is  $\sim 0.125 \text{ cm}^{-1}$  ( $\sim 0.01 \text{ nm}$ ). An inline fiber polarizer is used to control the polarization of the input light. For confirmation, a part of the transmitted light is used for polarization measurements. Simultaneously, the spectrum of the reflected light is measured using an optical multi-channel analyzer (OMA). The resolution of the OMA (QE65000, Ocean Optics) is  $\sim 2 \text{ nm}$ . The transmittance and reflectance values are calibrated using a CW Ti-Sapphire laser source (MBR-110, Coherent Inc.).

# 3. Results and Discussions

## 3.1. Nano-crater formation on nanofibers

For the fabrication, we vary the pulse energy, repetition rate and irradiation time (number of shots) to find the optimum conditions. It was found that for 1 kHz repetition rate, the nanofiber can be completely destroyed within 1 second, even at pulse energy of  $200 \text{ }\mu\text{J}$ . Even a repetition rate of 100 Hz can still seriously damage the nanofiber. However, we have found that by reducing the number shots to less than 20-shots, one could realize controlled nanofabrication on the nanofiber. By systematically changing the number of shots and pulse energy, we have found that single-shot irradiation is the best condition to realize clean nanofabrication. In the following, we discuss the fabrication results for multiple-shot and single-shot irradiation.

### 3.1.1. Multiple-shot fabrication

Figure 2(a) shows the SEM image of a typical sample fabricated by 20-shot irradiation with a pulse energy of  $370 \text{ }\mu\text{J}$ . We have found that many ablated structures are formed on the nanofiber. We must mention that these ablated structures are formed, not on the irradiation side, but on the

shadow side of the nanofiber. As one can see the ablation pattern is quite irregular. However, a crucial observation is that although the beam size along X-axis ( $60\ \mu\text{m}$ ) is much larger than the nanofiber diameter, the ablation pattern is formed in a line along the fiber axis (Z-axis).

Figure 2(b) shows the SEM image of a typical sample fabricated by 3-shot irradiation with a pulse energy of  $560\ \mu\text{J}$ . One can see rather regular and periodic ablation pattern is formed on the shadow side of the nanofiber. However, the ablated structures are elliptical and are elongated along the Z-axis. The typical size of an ablated structure is  $90\ \text{nm} \times 210\ \text{nm}$ . We must mention that such ellipticity is observed throughout the ablation pattern, even for the weakest ablated structure.

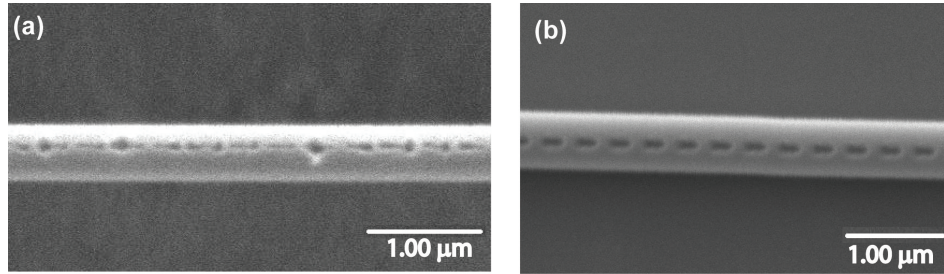


Fig. 2. (Color online) SEM images of samples fabricated by multiple-shot irradiation. (a) SEM image of a typical sample fabricated by 20-shot irradiation. (b) SEM image of a typical sample fabricated by 3-shot irradiation. The ablated structures are observed on the shadow side of the nanofiber.

### 3.1.2. Single-shot fabrication

Figure 3(a) shows the SEM image of a typical sample fabricated using single-shot irradiation with a pulse energy of  $630\ \mu\text{J}$ . As one can clearly see, periodic nano-crater structures are formed on the shadow side of the nanofiber. Such periodic structures are quite systematically formed over a length of few mm, consisting of thousands of such nano-craters. The inset shows the enlarged view of the sample. The shape of the nano-craters is almost circular and the diameter of a typical nano-crater is around  $210\ \text{nm}$ . The nano-craters are formed with a periodicity of  $350\ \text{nm}$ , which corresponds well to the interference fringe spacing. The depth of a typical nano-crater is measured by cutting the nanofiber at the nano-crater position and observing the cross-section using the SEM. The cross-sectional view is shown in Fig. 3(b). The nano-crater has a bowl-like shape and the depth is  $\sim 120\ \text{nm}$ .

### 3.1.3. Lensing effect of the nanofiber

It should be noted that the ablated structures shown in Fig. 2 and Fig. 3 are formed on the shadow side of the nanofiber. We could not observe any particular structure on the irradiation side. This suggests that the nanofiber itself acts as a cylindrical lens and focuses the femtosecond laser beam on its shadow surface [23, 24]. Also as shown in Figs. 2(a) and (b), the ablation pattern is formed exactly in a line along the fiber axis (Z-axis), confirming the lensing effect of the nanofiber. The uniqueness of the present method is that the lensing effect of the nanofiber makes it robust to any mechanical instabilities in the transverse direction (X-axis). But the instabilities along Z-axis can seriously affect the fabrication for multiple-shot irradiation, as the intensity pattern on the nanofiber may differ for each shot. This is evident from the observed irregular ablation pattern for 20-shot irradiation (Fig. 2(a)), where the periodicity is completely washed out due to the instabilities along Z-axis. Even for 3-shot irradiation (Fig. 2(b)) one can

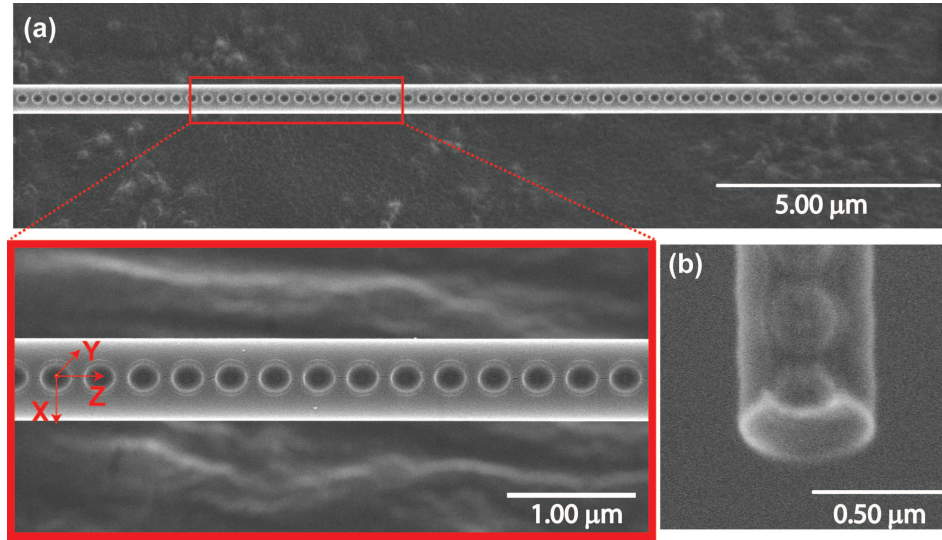


Fig. 3. (Color online) (a) SEM image of a typical sample fabricated using single-shot irradiation. The inset shows the enlarged view. The periodic nano-crater structures are observed on the shadow side of the nanofiber. (b) The cross-sectional image of a typical nano-crater measured by tilting the nanofiber at an angle of  $33^\circ$ .

see that the ablated structures are elongated along the fiber axis. However such instability does not affect the fabrication in single-shot irradiation as the irradiation time is only 120 fs (i.e. pulse length). As a result periodic nanostructures with well defined shape (shown in Fig. 3(a)) and periodicity are fabricated, without taking any special care to suppress mechanical vibrations. Moreover, such single-shot irradiation technique makes the fabrication method highly reproducible. The lensing effect of the nanofiber may explain the shape of the nano-craters. Although the field distribution along the Z-axis is limited by the interference pattern, the circular shape of the nano-craters is mainly due to focusing of the femtosecond laser along the X-axis.

### 3.2. Diameter distribution of nano-craters fabricated using single-shot irradiation

The diameter distribution of the nano-craters for two nanofiber samples, fabricated using single-shot irradiation, are plotted in Figs. 4(a) and (b), along with the corresponding nanofiber diameter. For Sample 1 the nano-craters are fabricated in the tapered region, and the diameter of the nanofiber varies from 500 nm to 680 nm. A periodic array of nano-craters is formed in a region exceeding 2 mm along the nanofiber axis. The diameter profile of the nano-craters shows a peak-like behavior and the  $1/e^2$  width is  $\sim 2.6$  mm. The diameter of the nano-craters varies from 95 nm to 290 nm. On the other hand, for Sample 2 the fabrication is done near to the waist region, and the diameter of the nanofiber is almost constant around 490 nm. The nano-craters are formed in a region of 0.8 mm along the nanofiber. The diameter of the nano-craters varies from 95 nm to 220 nm and the  $1/e^2$  width of the profile is  $\sim 1.03$  mm. The observations also suggest rather smaller depth of nano-craters for Sample 2 as compared to the Sample 1.

The observed  $1/e^2$  width of the diameter profile of the nano-craters is smaller than the original beam profile. This is due to the fact that the femtosecond laser induced ablation involves a multi-photon ionization process [25, 26]. Hence the ablation process scales as a higher power of the intensity and has some threshold condition. In order to understand the diameter profile of the nano-craters one must also consider the nanofiber diameter, as the lensing effect of

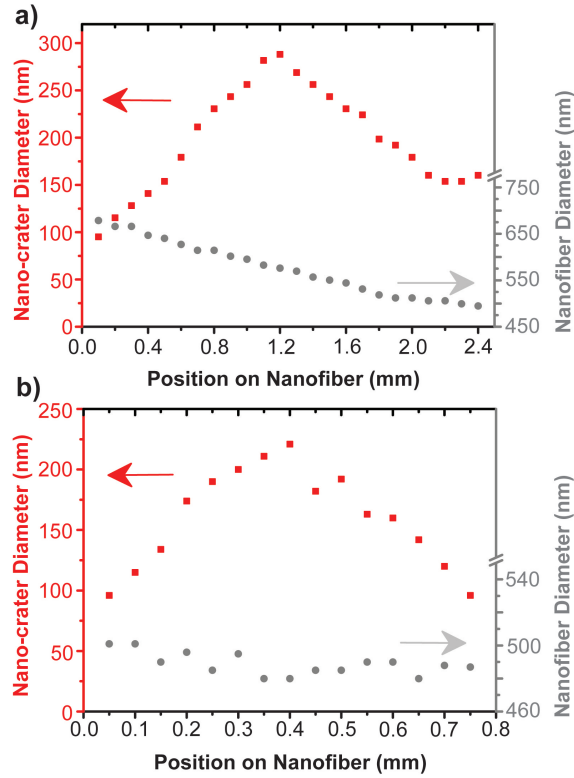


Fig. 4. (Color online) The diameter distribution of the nano-craters for two nanofiber samples, (a) Sample 1 and (b) Sample 2, fabricated using single-shot irradiation. The red squares denote the diameter of nano-craters and the gray circles denote the corresponding diameter of the nanofiber.

the nanofiber depends on the size parameter ( $2\pi a/\lambda$ ). In case of Sample 2, the reduction in the length of the nano-crater array and the smaller depths of the nano-craters may be understood from the decrease in the lensing effect of the nanofiber due to thinner diameter [23, 24]. The observation of nano-crater diameters down to 95 nm suggests that one can design various nanofabrications. The diameter distribution of the nano-craters can be designed by controlling the intensity distribution and the size parameter.

### 3.3. Optical properties of nanofibers with periodic nano-craters

Optical properties of the nanofiber samples, fabricated using single-shot irradiation, are characterized by measuring the transmission and reflection spectra. The transmission spectrum of Sample 1, shown in Fig. 5(a), shows a strong, broad reflection band centered around 825 nm. The FWHM of the reflection band is around 37 nm. In the wavelength region from 815 nm to 836 nm there is almost no transmission, indicating the stop band. The reflectivity values measured using a CW Ti-Sapphire laser confirms high reflectivity of 99% in this stop band region. The transmission and reflection spectra of Sample 2 are shown in Fig. 5(b). The transmission and reflection spectra are measured for two orthogonal linear polarizations, X-polarization (along X-axis) and Y-polarization (along Y-axis). The transmission spectrum for the X-polarization shows a reflection band centered around 823 nm and the FWHM is 10 nm.

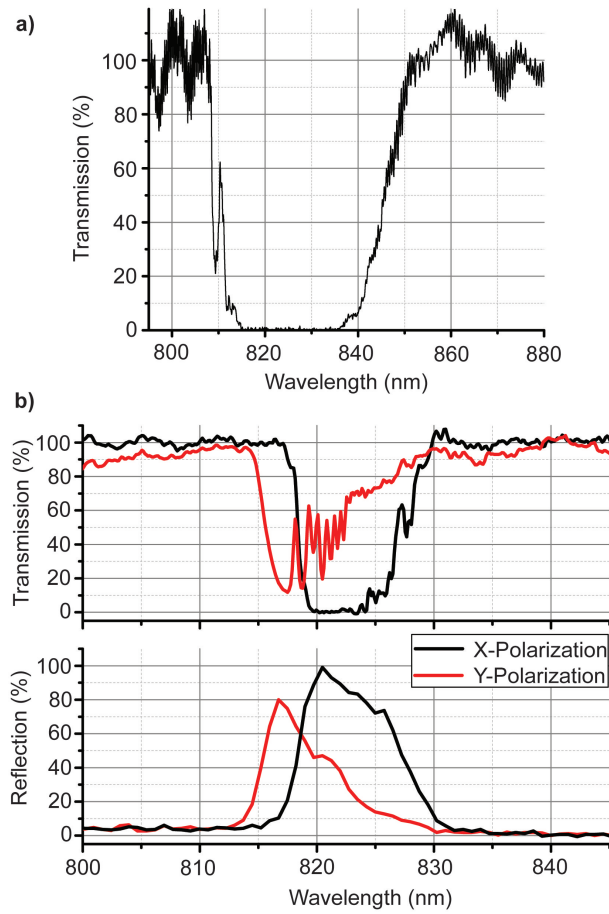


Fig. 5. (Color online) Optical characteristics of nanofiber samples fabricated using single-shot irradiation. (a) The transmission spectrum of Sample 1. (b) The transmission and reflection spectra of Sample 2, measured for two orthogonal polarizations, X-polarization (black curves) and Y-polarization (red curves).



The wavelength region from 819.5 nm to 824 nm denotes the stop band. Note that the transmission spectrum for the Y-polarization is blue shifted having a reflection peak at 817.5 nm and FWHM of 6.8 nm. The spectrum is asymmetric and shows several small sharp peaks in the red side. The reflection spectra almost match to the reflection band in the transmission spectra except that the fine features are washed out due to the resolution limit for the reflection measurements. The peak reflectivity values are measured using a CW Ti-Sapphire laser. For the X-polarization, we could observe almost 99% reflection in the stop band region, whereas for the Y-polarization the peak reflectivity is measured to be 80%.

The observation of high reflectivity values in the stop band region, clearly demonstrates that the periodic nano-craters on the nanofiber induce strong modulation of refractive index and act as a 1-D PhC. The observed spectral width for Sample 1 is 3.7 times broader than the Sample 2. This is mainly due to the nanofiber diameter variation for Sample 1, as the diameter determines the propagation constant and the Bragg resonance [27, 28]. In case of Sample 2, the observed blue shift for the Y-polarization may be explained using the same argument [27, 28]. Due to formation of nano-craters, the effective diameter along the Y-axis is reduced which results in such blue shift. Also the transmission spectrum for the Y-polarization is asymmetric and shows several small sharp peaks in the red side. Further investigations are required to understand such fine spectral features.

The peak reflectivity value for the Y-polarization is measured to be 80% whereas the transmittance value at this wavelength is 12.5%. This suggests that, for the Y-polarization, there is few percent scattering loss due to the nano-craters [27]. However, for the X-polarization, the scattering loss is negligible as is evident from the high transmittance values away from the stop-band region. One should expect high scattering loss as thousands of nano-craters are formed on the nanofiber. The observed low scattering loss and high reflectivity is mainly due to the shape and shallow depths of the nano-craters (shown in Fig. 3(b)). The observation of such excellent optical properties, clearly suggests that one can design various types of 1-D PhC cavities on nanofibers using the present fabrication method.

#### **4. Conclusion**

In conclusion we have demonstrated the formation of periodic nano-craters on a sub-wavelength diameter silica fiber using a femtosecond laser ablation technique. The ablation is achieved by irradiating only a single femtosecond pulse. Thanks to the lensing effect of the nanofiber, circular nano-crater structures are formed on the shadow surface of the nanofiber. Such a fabrication method may open new prospects in nanophotonics and nanofabrication technologies. We have demonstrated that the periodic nano-craters on the nanofiber act as a 1-D PhC. The PhC nanofiber system can become a promising workbench for quantum non-linear optics and will open new avenues in quantum information technology, by combining with laser-cooled atoms or solid-state quantum emitters. Also the PhC nanofibers may open up exciting new applications in lasing, optical switching and chemical/biological sensing.

#### **Acknowledgements**

We are thankful to Mark Sadgrove and Makoto Morinaga for fruitful discussions. Also we wish to thank Hitachi High-Tech Corp., Japan, for helping in SEM measurements with SU8040. This work was supported by the Japan Science and Technology Agency (JST) as one of the Strategic Innovation projects.